22nd ONERA-DLR Aerospace Symposium
1st - 3rd June 2022 - Hamburg, Germany

Basic Maneuver Load Alleviation in Conceptual Aircraft Design

Markus D. Krengel

Abstract Evaluating load alleviation technologies in conceptual aircraft design requires a cross-disciplinary simulation approach. In particular the design framework has to include a coupled, physics-based consideration of the disciplines aerodynamics, structures and flight dynamics rather than handbook equations. An approach like that enables the identification of possible overall aircraft efficiency benefits with active load alleviation. This paper presents a process that complies with the required level of fidelity, integrating flight control and aero-elasticity into the conceptual aircraft design. The software ASWING[1] is included and provides an unsteady lifting-line calculation combined with non-linear Euler beam theory. It is evaluated how aerodynamic load reduction and wing geometry layouts affect the overall aircraft design. The aircraft design is, in contrast to the more detailed wing sizing, based on handbook methods. Maneuver load cases are evaluated. A combined fuel consumption of three flight missions is the main parameter for the evaluation. Geometrical constraints for the tank volume and the span limit are discussed. A simplified, so-called 2.5D- method sizes the wing box based on a carbon-fiber-reinforced polymer topology. The design space contains up to 1008 aircraft designs varied in six design parameters. This set of aircraft design points is evaluated without any and with maneuver load alleviation. The findings show a combined maximum load alleviation and shape optimization potential in fuel burn of 17.6 % without further constraints. For the constrained design space the maximum fuel benefit is 11.4 % compared to the reference aircraft.

Keywords Aircraft Design · Load Alleviation · Aeroelasticity · CFRP

Markus Dino Krengel
DLR e.V., Institut für Aerodynamik und Strömungstechnik, Braunschweig
E-mail: markus.krengel@dlr.de

[1] Provided by the Massachusetts Institute of Technology (MIT) [6,7]

Nomenclature

AR	aspect ratio
b	wing span
c	chord
EAS	Equivalent Air Speed
η_{kink}	span-wise position of wing kink
$(M/S)_{max}$	maximum wing load
mTOM	maximum take-off mass
m_{wing}	total wing mass
ϕ_{LE}	wing leading edge sweep
TR	wing taper ratio
R	mission range

1 Introduction

A multidisciplinary wing design with load alleviation technologies requires at least the combination of three disciplines: aerodynamics, structures and flight dynamics in a coupled approach. In the early stage so-called "high fidelity" approaches based on unsteady Reynolds-Averaged Navier-Stokes equations coupled with structural finite element methods can usually not be applied because the required detailed geometric shapes are often not yet defined. Once the geometry is detailed enough, the available design space is already narrowed significantly. Haghighat, Martins, and Liu [12,13] showed large benefits for a higher endurance UAV, including an aeroelastic approach in the early design phase with a constrained wing optimization. Xu and Kroo [28] assessed a short-range aircraft including a flexible wing. They used the aircraft design environment PASS [19]. A simplified, physics-based viscous and aeroservoelastic model was included. The design did not contain an iteration of take-off weight for the design mission. Load alleviation and laminar flow technologies for the wing were included. They showed a fuel burn reduction of 11 % for a fully turbulent wing. Krishnamurthy and Luckner [20] integrated flight control laws and structural flexibility into the aircraft design with a focus on flight control. Still, a significant impact of the structural flexibility in early stage design was shown. These findings align with the results from Binder et al. [3]. They showed the combined effects of maneuver (MLA) and gust load alleviation (GLA), as well as passive structural tailoring (PST) for a long-range aircraft. MLA alone reduced the loads already 72 % of the maximum load reduction potential achieved with all three mechanisms combined. Wunderlich et al. [27] showed a "high fidelity" approach integrating load alleviation into wing design for a long range aircraft. The process chain was developed in the DLR-Project *VicToria* [11]. This approach had no feedback of the detailed wing design into an overall aircraft design environment due to the massive computational wall clock time required. Instead, some major overall aircaft geometry constraints were included and the wing mass change was connected to the payload. This ensured a constant wing loading. The optimized wing geometry with MLA resulted in a fuel burn reduction of 12.9 % for a highly flexible wing.

Here ASWING from Drela [6,7] is included as a physics-engine, integrating the flexible aircraft in a design framework. The load cases are based on design mission points. The process is demonstrated for a generic long-range transport aircraft with the technology level of the year 2020. Maneuver load alleviation is included via deployed flaps. The investigations are carried out within a multi-dimensional design space of overall aircraft parameters. It is explicitly not a full loads process including the whole load envelope which on the other hand usually cannot consider the design perspective adequately [22,16]. The process here is based on earlier activities [17,18]. The conversion problems described in Krengel and Hepperle [18] were reduced by including and adjusting relaxation factors.

2 Methodology of the Process

This paper utilizes a framework for conceptual aircraft design with a physics-based, flexible wing structure sizing. The framework is based on the DLR overall aircraft design environment OpenAD [26]. The open source CPACS file scheme [21,23,1] is the exchange database structure within the framework. This file exchange format is developed since the year 2005 and continuously updated by DLR [4]. Fig. 1 shows the general structure and data flow of the framework.

The input for the entire process contains a set of Top Level Aircraft Requirements, geometrical constraints for the planform, calibra-

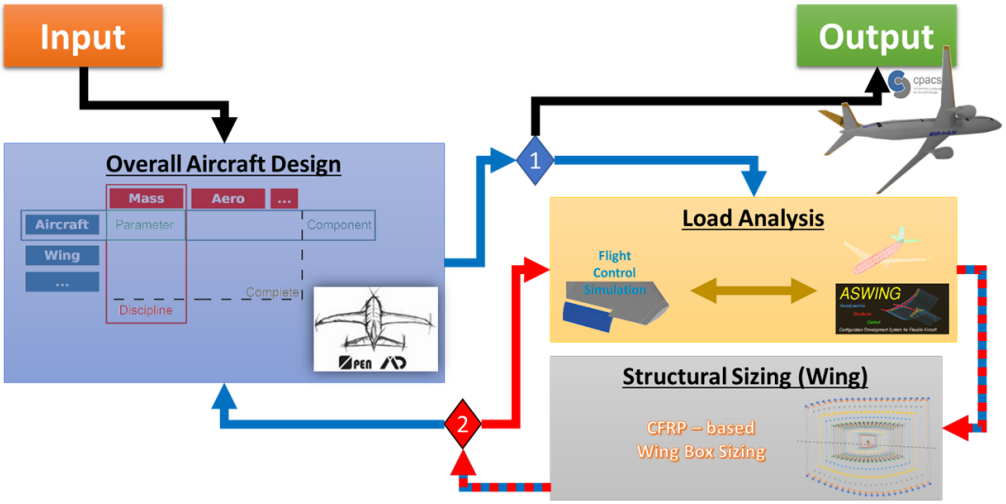

Fig. 1: Overview over the entire process flow for dynamic aeroelastic wing sizing.

tion factors and other assumptions, that are not covered by the level of physical representation. The global output is a CPACS file of a converged aircraft design, including a more detailed wing due to a physics-based sizing. Within the process two major loops, indicated with "1" and "2" in Fig. 1, cascade into each other.

The outer loop (**1**) feeds the wing mass and also a better estimation for the aerodynamic efficiency into the overall aircraft design. The aerodynamic update is from the ASWING lifting-line approach while the wing mass is a result of the sizing process shown in subchapter 2.4. Aircraft components like the landing gears or tail plains change in accordance with the handbook methods implemented in OpenAD [26].

The inner loop (**2**) computes the stiffness and mass distributions of the main wing where the loads are dependent on the wing's stiffness and mass and vice versa. Within this part, the output of ASWING is modified. Instead of the integrated value for induced drag directly on the vortices the more precise Trefftz-Plane analysis is used.

2.1 Design Space

The design space here is multi-dimensional. Besides the wing aspect ratio AR, taper ratio TR and the leading edge sweep Φ_{LE}, the relative span-wise position of the kink η_{kink}, the wing loading $(M/S)_{max}$ and the root chord length c_{root} are varied. Table 1 shows the design space steps for each of the six dimensions creating a study point mesh. The values of the reference aircraft design point are printed in bold. This results in a total number of 1 008 possible aircraft designs within each design study. For this investigation two studies

Table 1: Selected Design Space

Dim.	Parameter	Abbr.	Unit	Steps
1	Aspect Ratio	AR	-	8; 9, **9.92**; 10 12; 14; 16
2	Taper Ratio	TR	-	**0.199**; 0.3
3	LE Sweep	Φ_{LE}	°	30; **32**; 34
4	Root Chord	c_{root}	m	9.5; **10.6**; 12; 14
5	Kink Position	η_{kink}	-	**0.34**; 0.4; 0.45
6	Wing Loading	$(M/S)_{max}$	$\frac{Kg}{m^2}$	**672.3**; 600

are analyzed resulting in a total number of 2 016 possible aircraft design:

- one without any load alleviation, further labeled as **noLA**,
- and one with maneuver load alleviation, labeled as **MLA**.

2.2 Load Cases

A set of aero-elastic load cases is calculated for the structural sizing of the wing. The load cases are based on the design mission completed by a dive Mach number case. The dive Mach number is 0.07 higher than the cruise Mach number [8], as a simplified estimation. The process takes four flight points into account that are presented in Table 2. EAS represents the Equivalent Air Speed in knots, flaps up referrers to a clean wing configuration and flaps down represents a high-lift point.

Table 2: Flight Points Selected for Loads Calculation

No.	Mach	Altitude	EAS [kts]	FLAPs
1	0.83	10 668	266.32	UP
2	0.58	5 462	271.57	UP
3	0.9	10 668	288.75	UP
4	0.2	100	131.51	DOWN

For each flight point several maneuver load cases are calculated in accordance with federal regulations [8,9]. Symmetric maneuvers are simulated with a pull-up and pull-down case. Trimmed roll maneuvers are calculated with a bank angle of 30° and a corresponding maximum load factor of 1.67 [8]. Fig. 2 shows the considered load cases within the flight envelope after 14 CFR Part 25 [9]. Only maneuver load cases are taken into account for this investigation.

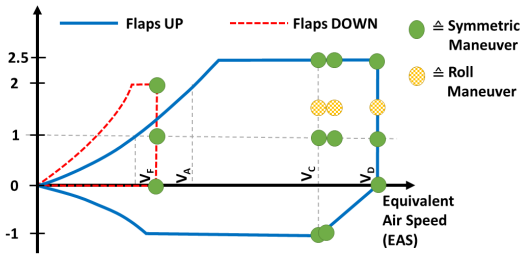

Fig. 2: Considered load cases for the analysis.

2.3 Maneuver Load Alleviation

The maximum deflection angles for MLA are given in Table 3 and are based on Wunderlich et al. [27]. To account for a roll control margin and to reduce the risk of control reversal the outer aileron is reduced in maximum deflection angle compared to the inner one by 25 %.

Table 3: Maximum Deflection of Movables

Movable	Max. Deflection
Inner Flap	+16.0 °
Outer Flap	−19.0 °
Inner Aileron	−20.0 °
Outer Aileron	−15.0 °

The flight control system here is a function based on the flight point equivalent airspeed (EAS) and the commanded load factor n_z. As indicated in Eq. 1, the commanded deflection for each movable is linearly dependent on EAS and the load factor. The maximum deflection aligns with a load factor of −1.0 (maximum delta to 1.0) or the dive velocity.

$$\delta_{movable} \propto \frac{EAS}{EAS_{Dive}} \propto \frac{n_z - 1}{2}. \quad (1)$$

2.4 Structural Sizing Model

The primary masses and the wing stiffness distributions are the output of a wing box sizing

model for carbon-fiber-reinforced polymers (CFRP). The 2D wing box representations are created by 10 equally distributed cuts along the wing span. The rib spacing is part of the structural stability calculation. Therefore, this method is considered a so-called 2.5-D approach. A topology optimization is not included. The number of stringers, the stringer foot and web geometry and laminate setup as well as the spars and skin element definition are set in the input file. The sizing is performed by multiplying each of the local laminate stack sequences by a natural number until all structural reserve factors are greater than 1.5. The calculation is done on a condensed representation shown in Fig. 3.

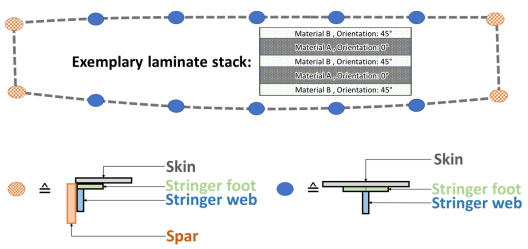

Fig. 3: Wing box sizing representation.

The original geometry of stringer and spars is condensed in points with "lumped" cross-sections. Each cross-section contains the original behaviour of the stringer connection. Reduced lumped areas are connected by webs with a shear stiffness of the original skin. This simplified model allows for a reserve factor calculation considering local skin and stringer buckling as well as global buckling and damage tolerance. The calculation is based on the laminate composite plate theory [24]. The resulting laminate stiffness matrix K_{lam} for each CFRP-laminate can be calculated from the extensional stiffness matrix A, the coupling stiffness matrix B and the bending stiffness matrix D as in:

$$K_{lam} = \begin{bmatrix} A & B \\ B & D \end{bmatrix} \quad . \tag{2}$$

The mid-plane strains ϵ^0 and mid-plane curvatures κ are connected to the resultant stress and moment vectors N and M by K_{lam}:

$$\begin{Bmatrix} N \\ M \end{Bmatrix} = K_{lam} * \begin{Bmatrix} \epsilon^0 \\ \kappa \end{Bmatrix} \quad . \tag{3}$$

The secondary wing mass is added to the sizing output by simple assumptions of average densities for the movables as well as the leading and trailing edges.

2.5 Target Parameter and Limits

The parameter for the aircraft design evaluation is a combined fuel consumption of three flight missions with a cruise Mach number of 0.83. The fuel consumption for each design mission is weighted by a factor w_i. Besides the design mission ($w_i = 0.3$), a mission with 75% design payload and a range of 4000 NM ($w_i = 0.55$) and a mission with maximum payload for a range of 2000 NM ($w_i = 0.15$) are considered. The fuel consumption for the two missions can be derived from a basic analytic mission approximation and the known mission fuel of the design mission. This analytic approximation is based on the mass ratio for the take-off (0.997), climb (0.981), descend (0.998) and landing segment (0.997) in Jenkins [15] as well as the Breguet equation [2] for the cruise segment. As long as the drag-lift-ratio cD/cL, the flight velocity v and the reserve fuel m_{rF} are constant, the fuel consumption for a mission F_m can be derived via:

$$F_m = [m_{OEW} + m_{PL} + m_{rF}] * \left(\frac{\frac{cD}{cL} \frac{R*g*sfc_{cr}}{v}}{\frac{0.981*0.997}{0.997*0.998}} - 1 \right) \quad ,$$

where m_{PL} is the pay load and R is the range. sfc_{cr} is the specific fuel consumption and m_{OEM} is the empty mass of the aircraft.

The aircraft designs will be discussed twice, without any limitation and with three limits constraining the valid design space:

- The mission loaded fuel fits inside the wing tank volume,
- The aircraft span b is smaller than a specific box limit,

– The available space behind the rear spar at the kink position is greater than a fixed percentage of the Mean Aerodynamic Chord.

2.6 The Reference Aircraft

The reference aircraft (REF) is a generic aircraft for long-range missions. It is designed to transport 270 passengers over a distance of 6000 nautical miles with a Mach number of 0.83. Some global aircraft parameters are shown in Table 4. The engine technology status is represented by the specific fuel consumption. Further indicated are the engine position in span direction and minimum static margin. In this case the aileron definition is set to a split aileron into an outer and inner aileron. The flap for high lift on the wing is also divided into an inboard and outboard flap. All flaps are modelled as plain flaps. The effect of these flaps regarding local pitching moment and additional lift are estimated via the formula of Glauert [10]. The main geometric dimensions are sketched out in Fig. 4.

Table 4: Selection of Global Parameter for the Overall Aircraft Design

Parameter	Description	Unit	Initial Value
Range	Design Range	[NM]	6000.0
Mach	Design Mach Number	[-]	0.83
mOI	Mass of Operator Items	[kg]	12 298.0
PAX	Number of Passengers	[-]	270
maxPL	Maximum Payload Mass	[kg]	31 050.0
mMisc	Additional (System) Mass	[kg]	0.0
sfc_{cr}	Specific Fuel Consumption in Cruise Point	[g/s/kN]	15.389
SM	Minimum Static Margin	[m]	0.2903
η_{Eng}	Engine Position along Span	[-]	0.3017
AilDef	Tuple[4] for the Geometry of Ailerons	[-]	
CalF	Tuple[4] for Mass and Drag Calibration Factors	[-]	

Further parameters define specifically the wing. These parameters are shown in Table 5. The $CFRPdef$ tuple[4] defines the topology of the carbon-fiber-reinforced polymers (CFRP) within the main wing box.

[4] Finite sequence of elements

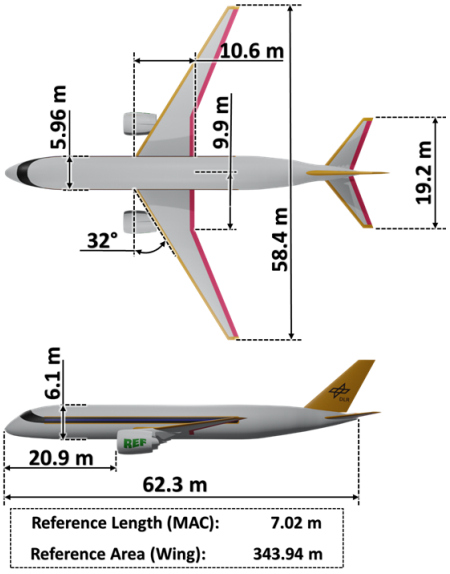

Fig. 4: Reference aircraft geometry.

Table 5: Selection of Wing Specific Parameters Defining the Geometry

Parameter	Description	Unit	Initial Value
$(M/S)_{max}$	Wing Loading at MTOW	$[kg/m^2]$	672.5
η_{Kink}	Kink Position of Main Wing	[-]	0.3399
ϕ_{LE}	Leading Edge Sweep	[deg]	32.0
ϵ_{dih}	Dihedral Angle	[deg]	6.0
AR	Aspect Ratio	[-]	9.92
TR	Taper Ratio	[-]	0.1992
C_{root}	Chord at Wing Root	[m]	10.63
SparDef	Tuple[4] for the Geometry of the Front and Rear Spar	[-]	
ALPHADef	Tuple[4] for Angle of Incidence	[-]	
TCDef	Tuple[4] for Airfoil Thickness	[-]	
CFRPdef	Tuple[4] for CFRP- Topology within the Wing Box	[-]	

3 Results

Subsequently, the major results of the study will be shown. In subchapter 3.1 the structural sizing results will be discussed exemplarily for the reference wing. Subchapter 3.2 shows a general overview of all aircraft designs within this study the subchapter 3.3 will filter the designs by the limits discussed above and

present the constraint optimum aircraft design with and without maneuver load alleviation.

3.1 Structural Sizing Results

Fig. 5 shows the skin thickness for all sections of the wing box sizing model. The front and rear spar as well as the lower and upper shell are shown. The left side of Fig. 5 represents the case without any load alleviation (noLA) and the right side the case with load alleviation active according to chapter 2.3.

Both cases show the maximum skin thickness in the middle sections 3-6 even though all thicknesses are reduced when MLA is active. Section 3, which is close to the engine position has a peak in skin thickness around the leading edge of the wing box and at the front spar. Further local peaks for both cases is the rear wing box part in section 4-6. The Case without load alleviation is reduced at the tip region to the minimum skin thickness down to section 9 ($\eta = 0.9$). Through load alleviation the region of minimum thickness is expanded to up to 20-30 % of the span ($\eta = 0.7 - 0.8$). In both cases the lower shell has a slightly higher skin thickness but for the MLA- case this is visible more clearly. The progression of thin thickness is plausible. There are no sudden jumps or discontinuities. The trend of higher thicknesses in the middle sections aligns with the findings in Wunderlich et al. [27] and Handojo et al [14]. The absolute thickness value though does not match entirely. The thicknesses here are below the skin thicknesses in Wunderlich et al. [27] but higher than the thicknesses in Handojo et al [14], where a smaller mid-range aircraft was investigated. Therefore, the magnitude of the skin thickness here is in a plausible range, in particular because it is highly dependent on the stringer and general topology of the (CFRP-)structure.

Fig. 6 shows the load case that has the lowest local structural reserve factor and therefore is locally sizing. Without load alleviation the dominant load case for the upper shell is the cruise pull-down maneuver at a load factor of -1, which is the load case with the highest speed at the lowest possible load factor. The lower shell as well as the spars are mainly sized by the pull-up equivalent which relates to the dive case. With activated load alleviation these load cases are reduced significantly. Instead some load cases are nearly equal in the resulting stresses which leads to higher number of relevant and dominant load cases. It is significant, that for the skins close to the trailing edge maneuver load cases with deployed flaps at low speed become sizing. That is also plausible because the flaps are bringing in loads at the rear end of the wing box and because the load alleviation is not very "aggressive" at low speed flight points. Therefore, high speed loads are reduced more than low speed loads.

3.2 Aircraft Designs without constraints

In a graph of the aerodynamic efficiency over the relative wing mass each aircraft design point can be placed. Fig. 7 shows the envelope of all these points once for the study with no load alleviation and once for the study with load alleviation. The diamond-shaped symbol represents the reference aircraft. The envelopes shape is a 2D-mapping of the six-dimensional design space for each investigation. Due to the discrete steps in the dominant root chord length the envelopes almost split between a root chord of 12 and 14 m. There are constant lines of root chord and aspect ratio values for the reference study (noLA) which form a pattern of almost perpendicular directions.

The lines of constant root chord show that an increasing aspect ratio leads to a better aerodynamic efficiency at the cost of a higher wing mass. The lines of constant aspect ratio on the other hand show a decreasing wing mass and an increasing aerodynamic efficiency with decreasing root chord length. This leads to a slimmer wing where the structure in the inboard area is increased in skin thickness in comparison to Fig. 5. Even though this trend is

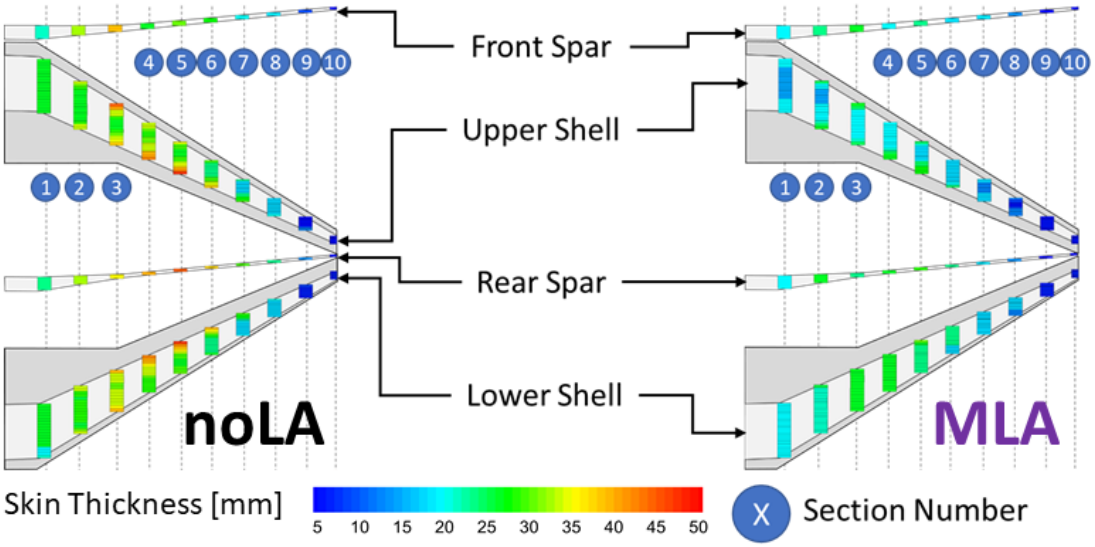

Fig. 5: Skin thickness in the sizing sections for the reference wing geometry with and without load alleviation.

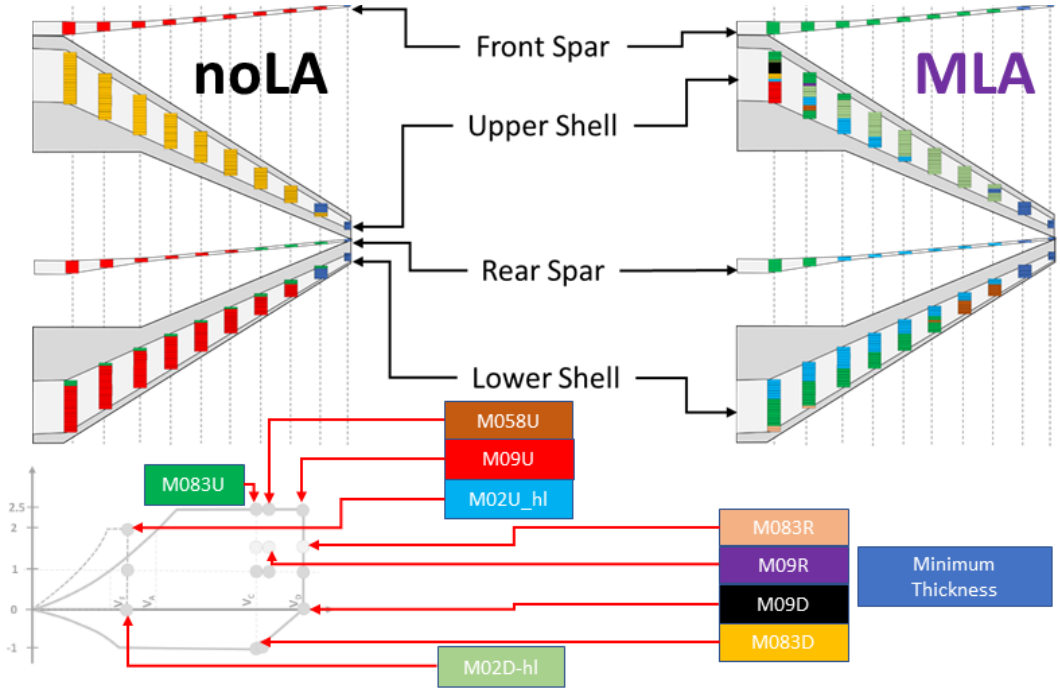

Fig. 6: Sizing load cases with and without load alleviation for the reference wing geometry.

preferable, Fig. 7 already indicates a decreasing effect because the lines of constant aspect ratio become denser. Previous studies already showed, that a root chord of 9 m is close to the possible minimum [18]. Furthermore, these previous studies showed, that for a root chord

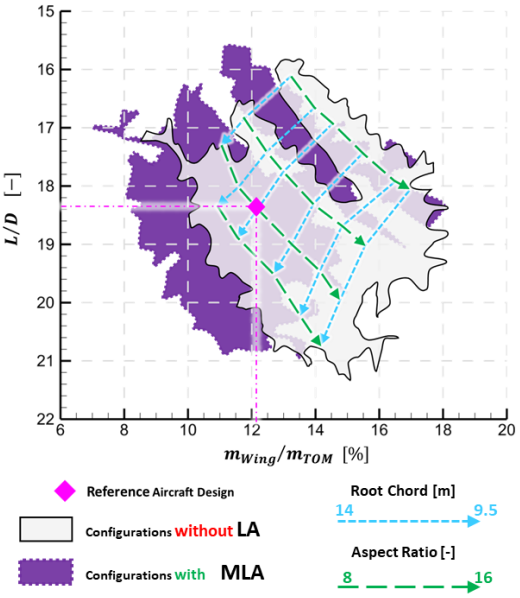

Fig. 7: Envelopes of all resulting aircraft design points with and without load alleviation.

length below 9.5 m the main landing gear cannot be integrated behind the wing box because the installation space is too small.

The envelope, representing the aircraft designs with MLA is shifted to lower relative wing mass values compared with the envelope without load alleviation. This is the consequence of a reduced primary wing mass. The secondary effect is a slight shift upwards to a lower aerodynamic efficiency. The wing stiffness is reduced and a higher wing bending occurs. Therefore, the aerodynamic efficiency is reduced.

3.3 Constrained Design Space and Optimum Aircraft Design

As mentioned in subchapter 2.5, there are reasonable limits to the entire design space within this study. The resulting aircraft designs can be filtered by these constraints yielding a much smaller number of valid aircraft designs according to these limits. Here, three limits are considered. The fuel volume inside the wing box is required to be larger than the mission fuel and the span limit is 65 m. To ensure, that flaps can be integrated properly the minimum installation space at the kink position behind the rear spar is constrained as well to ensure the effectiveness of the flaps. The effectiveness is not only dependent on the flap chord length but also on the spanwise expansion of the flap. Therefore, the limit is a percentage of the Mean Aerodynamic Chord. Here it is 15.5 %, which is 1.085 m for the reference aircraft.

Fig. 8 shows all aircraft designs fulfilling these constraints and moreover are more or equally efficient in combined fuel burn than the reference aircraft design. Each aircraft design is represented by a symbol in the graph. The combined fuel burn is indicated as a colour code and represents the combined mission fuel over the transport work carried out by the aircraft when transporting a specific payload over a certain distance. The optimum aircraft designs with and without MLA are also indicated within Fig. 8.

The number of valid and better designs in terms of fuel consumption raises in total from 80 to 112 when load reduction is considered. Load reduction makes more designs feasible and more efficient within the constrained design space. Besides the span limit, for aircraft designs without load alleviation mainly the fuel volume requirement is limiting. This limit could be shifted by allowing for an additional tank within the fuselage, which was not done here for comparison reasons. Aircraft designs with MLA are, besides the span limit, strongly limited by the installation space limit for the flaps. The aircraft designs are in large part lighter than without MLA and therefore reduced in wing reference area. Even though the limit is based on the mean chord, it still has this significant impact.

The optimum aircraft designs, indicated in Fig. 7 are shown in Table 6. The optimum with load alleviation tends to a wing with reduced root chord length. In total the combined fuel savings δm_{BF_c} are 8.4 % for the optimum

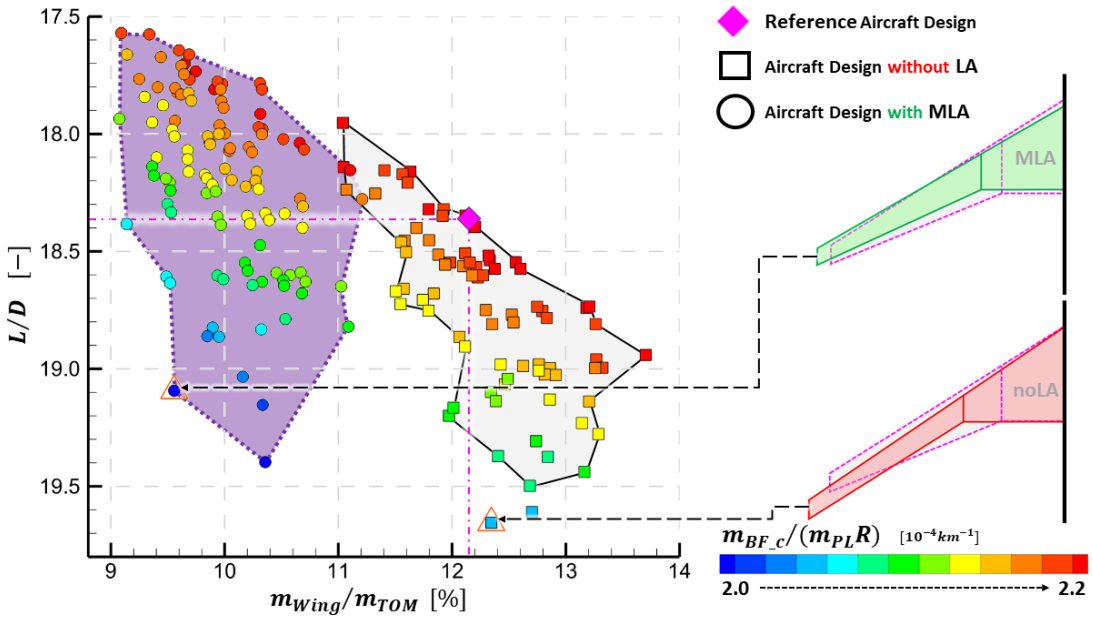

Fig. 8: Aircraft design points with and without load alleviation, fulfilling all defined constraints and are equal or more efficient than the reference aircraft design.

without load alleviation and 11.4 % for the MLA-optimum.

Table 6: Selected Design Space

ACD	AR	TR	Φ_{LE}	$(M/S)_{max}$	η_{kink}	c_{root}	δm_{BF_c}
REF	9.92	0.199	32	672.3	0.34	10.6	**0.0 %**
noLA	12	0.199	34	672.3	0.45	10.6	**-8.4 %**
MLA	12	0.199	30	672.3	0.40	9.5	**-11.4 %**

4 Conclusion and Outlook

This investigation utilized a process for the integration of physics-based, aero-elastic wing design into the overall aircraft design. The process utilizes the MIT software ASWING [6,7] to calculate aero-elastic load cases for a generic transport aircraft design. Load alleviation can be introduced in the load cases. The wing was sized as a CFRP- wing based on laminate composite plate theory. The DLR overall aircraft design environment OpenAD [26] was applied. In a six-dimensional design space of design parameter a number of up to 1 008 long-range aircraft designs have been investigated. The two-part investigation contained the same study points with and without maneuver load alleviation by wing trailing edge flaps. The resulting aircraft designs are filtered by several reasonable limits, yielding an optimum design for both study-parts based on the assessment of combined fuel consumption for three relevant study missions. As a result, the constrained fuel saving potential with maneuver load alleviation is 11.4 % compared to the reference aircraft design. The rather strict limits reduced the valid designs down to a share of 8-11 % beneficial designs within the original design space.

In future research this percentage could possibly be raised by adjusting the design space according to the presented findings. Furthermore, dynamic gust load cases will be considered as well as gust load alleviation. In

addition, the modelling of airfoil aerodynamics will be adjusted. So far, the assumptions along the span are based on the mean airfoil thickness. In the future it is planned, to use a more detailed approach based on the local profile thickness. Wunderlich et al. [27] showed a significant potential for the parameter of thickness distribution. For future work the process could include more than just OpenAD, like a design tool chain based on openAD via RCE [5,25].

Acknowledgements The author would like to thank Professor Mark Drela and the MIT for providing the ASWING research license.

References

1. Alder, M., Moerland, E., Jepsen, J., and Nagel, B., *Recent Advances in Establishing a Common Language for Aircraft Design with CPACS*, Aerospace Europe Conference 2020, Bordeaux, Frankreich, 2020. URL https://elib.dlr.de/134341/.
2. Anderson, J. D., and Bowden, M. L., *Introduction to flight*, McGraw-Hill Education, 2 Penn Plaza, New York, NY 10121, 2005.
3. Binder, S., Wildschek, A., and De Breuker, R., *The interaction between active aeroelastic control and structural tailoring in aeroservoelastic wing design*, Aerospace Science and Technology 110, 2021, pp. 1–12. doi:10.1016/j.ast.2021.106516 106516.
4. *CPACS Homepage*, https://cpacs.de, 2021. Accessed: 2022-04-25.
5. DLR, *Remote Component Environment (RCE)*, 2021. URL https://rcenvironment.de/.
6. Drela, M., *ASWING 5.99 Technical Description - Steady Formulation*, Massachusetts Inst. of Technology, Cambridge, MA, 2015, Chaps. 1, 8.
7. Drela, M., *ASWING 5.99 Technical Description - Unsteady Extension*, Massachusetts Inst. of Technology, Cambridge, MA, 2015, Chaps. 1, 15.
8. EASA, *Certification Specifications and Acceptable Means of Compliance for Large Aeroplanes CS-25 (Amdt. 17)*, European Aviation Safety Agency (EASA), Cologne, Germany, 2015.
9. FAA, *Code of Federal Regulations, Title 14 Part 25 (14 CFR 25) Airworthiness Standards: Transport Category Airplanes 14 CFR 25 - revised and re-issued annually*, 1988. Accessed: 2021-10-27.
10. Glauert, H., *Theoretical Relationship for an Airfoil with Hinged Flap*, ARC Rep. Mem. 1095, 1927.
11. Goertz, S., Abu-Zurayk, M., Ilic, C., Wunderlich, T. F., Keye, S., Schulze, M., Kaiser, C., Klimmek, T., Süelözgen, ., Kier, T., and Schuster, A., *Overview of Collaborative Multi-Fidelity Multidisciplinary Design Optimization Activities in the DLR Project VicToria*, AIAA Aviation 2020 Forum 2020, 2020, p. 3167. doi:10.2514/6.2020-3167.
12. Haghighat, S., Liu, H. H. T., and Martins, J. R. R. A., *Model-Predictive Gust Load Alleviation Controller for a Highly Flexible Aircraft*, Journal of Guidance, Control, and Dynamics, Vol. 35, No. 6, 2012, pp. 1751, 1766. doi:10.2514/1.57013.
13. Haghighat, S., Martins, J. R. R. A., and Liu, H. H. T., *Aeroservoelastic Design Optimization of a Flexible Wing*, Journal of Aircraft, Vol. 49, No. 2, 2012, pp. 432, 443.
14. Handojo, V., Lancelot, P., and De Breuker, R. *Implementation of active and passive load alleviation methods on a generic mid-range aircraft configuration.* 2018 Multidisciplinary Analysis and Optimization Conference (p. 3573). 2018. DOI: 10.2514/6.2018-3573
15. Jenkinson, L. R., Simpkin, P., Rhodes, D., Jenkison, L. R., and Royce, R., *Civil jet aircraft design (Vol. 338)*. London, UK: Arnold. 1999. ISBN: 0 340 74152 X
16. Kier, T. M., Verveld, M. J., and Burkett, C. W., *Integrated Flexible Dynamic Loads Models Based on Aerodynamic Influence Coefficients of a 3D Panel Method*, Proceedings of the IFASD 2015, 2015.
17. Krengel, M. D., Hepperle, M., and Huebner, A., *Aeroservoelastic Wing Sizing Using a Physics-Based Approach in Conceptual Aircraft Design*, AIAA Aviation 2019 Forum, 2019, p. 3368. doi:10.2514/6.2019-3368.
18. Krengel, M. D., Hepperle, M., *Effects of Wing Elasticity and Basic Load Alleviation on Conceptual Aircraft Designs*. AIAA SCITECH 2022 Forum, 2022, p. 0126. doi:10.2514/6.2022-0126
19. Kroo, I. M., *An Interactive System for Aircraft Design and Optimization*, AIAA 1992 Aerospace Design Conference, Vol. 92, 1992. doi:10.2514/6.1992-1190.
20. Krishnamurthy, V., Luckner, R., *Flight Mechanical Modelling considering Flexibility and Flight Control Functions in Preliminary Aircraft Design*, AIAA Modeling and Simulation Technologies Conference, Denver, Colorado, 2017, doi:10.2514/6.2017-4332.
21. Liersch, C. M., and Hepperle, M., *A distributed toolbox for multidisciplinary preliminary aircraft design*, CEAS Aeronautical Journal, Vol. 2, No. 1-4, 2011, pp. 57, 68. doi:10.1007/s13272-011-0024-6.
22. Looye, G., *Integrated Flight Mechanics and Aeroelastic Aircraft Modeling using Object-Oriented Modeling Techniques*, Modeling and Simulation Technologies Conference and Exhibit, 1999. doi:10.2514/99-4192.
23. Nagel, B., Böhnke, D., Gollnick, V., Schmollgruber, P., Rizzi, A., La Rocca, G., and Alonso, J., *Communication in aircraft design: Can we establish a common language*, 28th International Congress of the Aeronautical Sciences, 2012, pp. 1,13.
24. Roylance, D., *Laminated composite plates*, Massachusetts Institute of Technology (MIT), Cambridge, 2000.
25. Seider, D., Litz, M., Schreiber, A., Fischer, P. M., and Gerndt, A., *Open source software framework for applications in aeronautics and space*, IEEE Aerospace Conference, 2012, 2012, pp. 1, 11. doi:10.1109/AERO.2012.6187340.
26. Woehler, S., Atanasov, G., Silberhorn, D., Fröhler, B., and Zill, T., *Preliminary Aircraft Design within a Multidisciplinary and Multifidelity Design Environment*, Aerospace Europe Conference 2020, Bordeaux, Frankreich, 2020. URL https://elib.dlr.de/140902/.
27. Wunderlich, T. F., Dähne, S., Reimer, L., and Schuster, A., *Global Aerostructural Design Optimization of More Flexible Wings for Commercial Aircraft*, Journal of Aircraft, 2021, pp. 1, 18. doi:10.2514/1.C036301
28. Xu, J., and Kroo, I., *Aircraft Design with Active Load Alleviation and Natural Laminar Flow*, Journal of Aircraft, Vol. 51, No. 5, 2014, pp. 1532, 1545. doi:10.2514/1.C032402.